

# AViNet: Diving Deep into Audio-Visual Saliency Prediction

Samyak Jain<sup>1</sup> Pradeep Yarlagadda<sup>1</sup> Ramanathan Subramanian<sup>2</sup> Vineet Gandhi<sup>1</sup>

<sup>1</sup>CVIT, Kohli Centre on Intelligent Systems, IIT Hyderabad <sup>2</sup>IIT Ropar

samyak.j@research.iiit.ac.in pradeep.yarlagadda@students.iiit.ac.in

## Abstract

We propose the *AViNet* architecture for audiovisual saliency prediction. *AViNet* is a fully convolutional encoder-decoder architecture. The encoder combines visual features learned for action recognition, with audio embeddings learned via an aural network designed to classify objects and scenes. The decoder infers a saliency map via trilinear interpolation and 3D convolutions, combining hierarchical features. The overall architecture is conceptually simple, causal, and runs in real-time (60 fps). *AViNet* outperforms the state-of-the-art on ten (seven audiovisual and three visual-only) datasets, while surpassing human performance on the CC, SIM and AUC metrics for the AVE dataset. Visual features maximally account for saliency on existing datasets with audio only contributing to minor gains, except in specific contexts like social events. Our work therefore motivates the need to curate saliency datasets reflective of real-life, where both the visual and aural modalities complementarily drive saliency. Our code and pre-trained models are available at <https://github.com/samyak0210/VideoSaliency>

## 1. Introduction

Video saliency prediction focuses on understanding and modeling human visual attention (HVA) while viewing a dynamic scene. Upon compiling the *ground truth* regarding where viewers gaze in the scene via eye-tracking hardware, saliency prediction (SP) aims to computationally mimic HVA given a novel video. SP is useful for prioritizing visual information across space and time, and finds value in a variety of applications like video summarization [21], stream compression [15], video surveillance [13], video captioning [29], cinematic editing [28], video retargeting [31], etc.

Video SP models primarily employ visual information to predict gaze. Larger datasets like *DHF1K* [44] discard audio during ground truth collection, and ask users to look at *silent* videos. End-to-end deep saliency models are then trained using only visual information. State-of-the-art video SP models largely depend on Long Short-



Figure 1. The core of our approach is a strong visual-only model ViNet. Here, we compare ViNet (third column) with state-of-the-art UNISAL model [12] (fourth column). Note that ViNet better captures the action, while UNISAL focuses on objectness. In this example, ViNet focuses on the region being drawn, whereas UNISAL focuses on completed portion. Best viewed in color and under zoom.

Term Memory (LSTM) networks to encode temporal dependencies [12, 45, 20]. These models build on image-based saliency, and aggregate frame-wise prediction using an LSTM. Since both spatial decoding and temporal aggregation are performed separately, LSTM models are unable to collectively leverage spatio-temporal information, shown to be beneficial for video SP [24].

More fundamentally, discarding audio information contrasts with our real-life behavior, where we perceive visual and audio modalities simultaneously. Cognitive studies confirm that auditory and visual cues are correlated and jointly contribute to human attention [40]. Consequently, recent efforts have explored multi-modal (audio-visual) video SP [37, 39], and demonstrate audio as a strong SP cue. We dive deeper into audio-visual SP, comprehensively analyzing ten saliency datasets.

We propose a novel audio-visual saliency prediction model called AViNet. AViNet takes a set of frames as input and predicts a saliency map for the last frame. Following the methodology adopted in [24], it then employs a sliding window approach to predict saliency for the entire video. A vision-only fully convolutional encoder-decoder, termed

ViNet, forms the core of our architecture. ViNet takes features learned from an action recognition network from multiple hierarchies, fuses them in a UNet [33] like fashion, and outputs a saliency map using trilinear interpolations and 3D convolutions. ViNet surpasses the state-of-the-art on three of the popular vision-only saliency datasets (a motivating example is illustrated in Figure 1). ViNet is also the top-ranked on the private test-set of *DHF1K*, the most diverse saliency benchmark <sup>1</sup>.

We then augment ViNet with an audio branch. The resulting AViNet architecture fuses audio and visual information to predict audio-visual saliency. AViNet is end-to-end trainable, and uses pre-trained audio features from SoundNet [3]. We explore three different fusion strategies, *i.e.*, simple concatenation, bilinear fusion, and transformer based fusion. AViNet improves significantly over ViNet on the Coutrot2 dataset [10], which focuses on social event scenarios (conversations among multiple persons). There are nil or marginal improvements on the other five audio-visual SP datasets. Our results suggest that current audio-visual saliency models [37, 39] are not optimal on the visual modality, and hence exaggerate the contributing role of audio.

Overall, we make the following research contributions:

- We propose a novel visual-only architecture called ViNet for video saliency detection. The architecture is conceptually simple and backed by thorough ablation studies. We further augment ViNet with audio features, resulting in an audio-visual model called AViNet. We explore three different fusion mechanisms.
- We present a comprehensive analysis on ten different datasets. Our model significantly outperforms the state-of-the-art on three visual and seven audio-visual datasets.
- We carefully explore the role of audio and find that the visual-only model almost recovers the underlying performance. This motivates the need for carefully curated datasets for evaluating audio-visual saliency.

## 2. Related Works

### 2.1. Video Saliency

The recent landscape in video saliency prediction is dominated by the end to end trainable deep networks. The availability of large datasets like Hollywood-2 [22] and *DHF1K* [44] have been instrumental in this progress. Hollywood-2 is the largest dataset, however, its content is limited to human actions and movie scenes. *DHF1K*

is considered the most diverse and challenging dataset for saliency detection.

Majority of the recent approaches rely on an LSTM based architecture for sequential fixation prediction over successive frames. Wang *et al.* [44] combine frame-level image features using a ConvLSTM. SaLEMA [20] model recurrence using a temporal exponential moving average (EMA) operation over the convolutional layer. They show such a simple moving average based approach matches the performance achieved using a ConvLSTM. SALSAC [45] adds further complexity to basic convLSTM architecture through a shuffled multi-level attention module and a frame correlation module. STRA-Net [7] learns an alignment module, and then aligned frames are sent into a Bi-ConvLSTM. [16] propose a novel construction of LSTM (2C-LSTM) with two sub-networks to focus on objectness and motion, respectively. UNISAL [12] is a unified image and video saliency prediction model that uses MobileNet to extract spatial features and LSTMs for encoding temporal information. The method heavily relies on domain adaptive prior maps (different prior maps for image and video domains), domain adaptive batch-normalization, etc. Several of these video saliency prediction architectures [12, 44] borrow and extend ideas (hierarchical features, transfer learning, multi-branch architectures, etc.) from the models trained for static image saliency prediction [17, 32].

3D convolutional architectures have also been explored for the task. These methods typically rely on action detection networks as their backbone. TASED-Net [24] uses S3D as an encoder to extract spatial features while jointly aggregating all the temporal information in order to produce a single full-resolution prediction map. They use transposed convolution layers, with auxiliary pooling ( a variation of max-unpooling layers) for spatial upscaling in the decoder. Bellitto [6] et al. use multiple decoders for features encoded at different levels to obtain multiple saliency instances that are finally combined to obtain final output saliency maps. [6] is inspired by the DVA image saliency model [43]. A combination of 3D convolutions and recurrent architecture has also been explored [5]. STSConvNet [4] explicitly computes optical flow and fuses the optical with the visual features into two-stream convolutional architecture.

In contrast, our ViNet method is a conceptually simple encoder-decoder architecture exploiting basic ideas of spatial hierarchy, feature concatenation, skip connections, trilinear upsampling, and 3D convolutions. It does not use any dataset priors, it does not need any explicit input like optical flow, and also avoids any extra modules for detecting objectness, motion, attention, etc. It still outperforms state of the art by a reasonable margin and motivates the need to step back and exploit simpler alternatives before proposing more complex ones.

<sup>1</sup><https://mmcheng.net/videosal/>

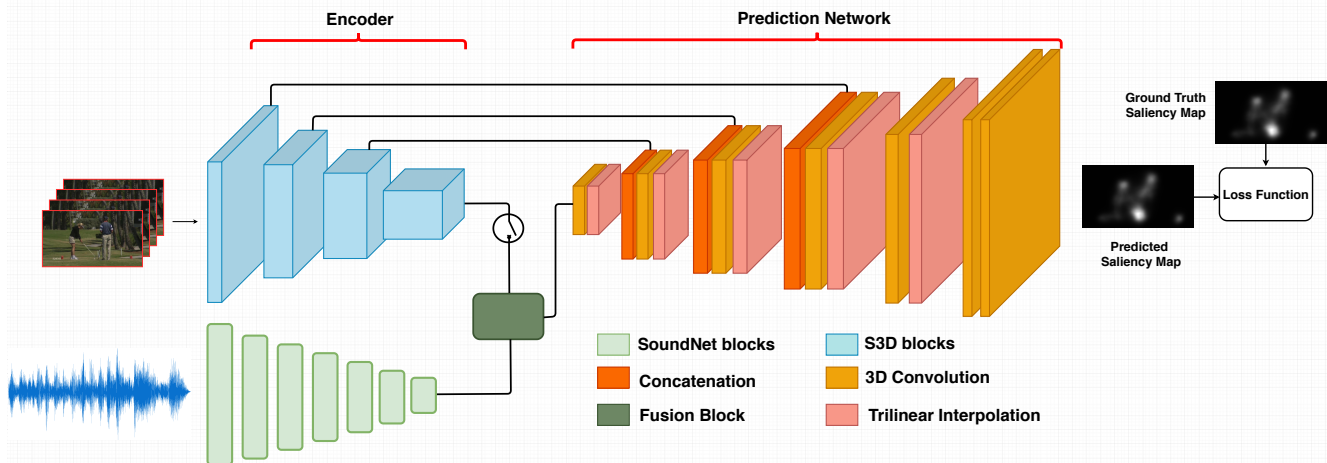


Figure 2. AViNet Architecture overview.

## 2.2. Audio-Video Saliency

Research in cognitive neuroscience has led to interesting findings about audiovisual integration. If you ever watched a ventriloquist in action, you would agree how they trick our visual stimuli to guide the perceived location of the sound (and where we look at). Ventriloquist turns to face the puppet, they attend the puppet, use a different voice for the puppet, and make it seem that it is the puppet that is talking (although the sound is being generated from their stomach). McGurk effect [23], pip and pop effect [41], unity assumptions [42] are other examples of how we jointly integrate and perceive visual and audio modalities. Coutrot et al. [11, 9, 10] present some interesting studies on the influence of soundtrack on eye movements during video exploration.

Application-specific attempts have been made for visual saliency and audio localization [34, 35, 8]. The fusion of handcrafted attention models and pre-trained deep image-level models using canonical correlation analysis has been explored [25, 26]. However, only a couple of attempts have been made towards an end to end deep learning-based audio-visual saliency fixation prediction. Tavakoli [37] et al. trains two independent networks for the two modalities (audio and visual data), and their outputs are simply concatenated as a late fusion scheme. They use 3DResNet as the backbone for both modalities. STAVIS [39] extends the SUSiNet [19] visual saliency model and investigate three different ways to fuse the audio modality.

Significant efforts have been made in the direction of self-supervised learning and representation learning exploiting audio-visual data. SoundNet [3] leverage the natural synchronization between vision and sound to learn an acoustic representation. They use a student-teacher training procedure to transfers discriminative visual knowledge (large scale visual recognition) into the sound modality.

On similar lines, audiovisual correspondence has been exploited for the task of cross-modal retrieval [2], sound classification [3, 1], sound localization in images [2, 36], scene analysis [30], temporal event localization [38] etc.

## 3. Proposed Architecture

We propose an end-to-end architecture visual-only model called ViNet. It is a fully 3D-convolutional encoder-decoder architecture that predicts the saliency for the last frame of the corresponding set of sequential frames. Then we present an audio-visual saliency detection model called AViNet that fuses the visual features from ViNet and audio features from SoundNet. Fig.2 displays an overview of the architecture.

### 3.1. Backbone

The architecture uses the S3D network [46] as the video encoder. We use the model pre-trained on the Kinetics dataset which is an action-recognition dataset. We use S3D since it consists of 3D convolutional layers which efficiently encodes the spatio-temporal information. Moreover, it is light-weight and pre-trained on a big dataset, makes it fast and effective for transfer-learning. It consists of 4 convolutional blocks base1, base2, base3 and base4 that provides outputs  $X_1, X_2, X_3$  and  $X_4$  in different spatial and temporal scales.  $X_1, X_2$  and  $X_3$  are referred as multi-level features that are extracted at three-levels of hierarchy. The input to the encoder is a clip  $x_{clip} \in R^{3 \times T_0 \times H_0 \times W_0}$ , where  $T_0$  is 32. It generates a lower-resolution activation map  $X_4 \in R^{C \times T \times H \times W}$ , where  $C = 1024$  and  $T, H, W = \frac{T_0}{8}, \frac{H_0}{32}, \frac{W_0}{32}$ .

For audio representation, we employ SoundNet [3], which is a 1D fully-convolutional network, rather than using 2D CNNs to encode time-frequency representation. It consists of seven layers of 1D convolutions and max pool-

ing. It is pre-trained on a large amount of sound data collected in the wild, making it efficient in sound localization tasks. Firstly, the audio is cropped in accordance with the duration of the visual frames, i.e., 32 frames, by taking into account the frame rate of video and sampling rate of audio. Since the frame and sampling rate of videos and corresponding audio can vary, we chose this network because of its ability to handle variable-length audio. We apply similar pre-processing of audio information defined by SoundNet. We normalize the audio values and apply Hanning window operation in order to weigh the higher central audio values representing the current time instance, but also include past and future values with attenuation. The sound module takes 1D pre-processed audio feature as input,  $y_{audio} \in R^{1 \times \hat{T} \times 1}$  and outputs audio features  $A \in R^{1024 \times 3 \times 1}$ .

### 3.2. Audio Visual Fusion

We explore three types of fusion techniques. First is a simple concatenation of encoded audio and video features. We repeat the audio features to match the dimensions of visual features and combine them across the channel dimension. Then we apply  $1 \times 1$  Convolution to reduce the number of channels.

Secondly, we applied bilinear fusion where the visual features are first passed through Max Pool to reduce the spatial and temporal dimension and then collapsed to represent it as a vector  $x_1 \in R^{1024 \times x_0}$ . Similarly, the audio features are collapsed as a vector  $x_2 \in R^{1024 \times y_0}$ . The bilinear fusion is defined as

$$y = x_1^T A x_2 + b \quad (1)$$

where  $A \in R^{x_0 \times x \times y_0}$  and  $b \in R^{x \times 1}$  are parameters and  $x$  is the desired output dimension.

The third method we explore is transformer-based fusion. The visual and audio features are passed through  $1 \times 1$  Convolution to reduce the number of channels. Then, the spatial and temporal dimension is collapsed for both and concatenated along the channel dimension. Each feature vector of fused output is passed through the transformer encoder as a sequence to apply self-attention between both features. Since the size of the transformer’s output is the same as the input, we split it into two vectors, just like before they were fused. But now the visual features have attended over audio features and vice-versa. The second dimension of the visual-attended audio feature is collapsed by taking mean over them and tiled across new visual features.

### 3.3. Prediction Network

The Prediction Network consists of 6 decoding layers  $D_1, D_2, D_3, D_4, D_5$  and  $D_6$  which output  $O_1, O_2, O_3, O_4, O_5, O_6$ . The layers  $D_2, D_3$  and  $D_4$  consists of one concatenation, 3D convolutional and tri-linear upsampling layer to fuse multi-level feature and match the dimension of features

Model Architecture	CC	SIM	NSS
Without Hierarchy	0.5002	0.361	2.7371
With Hierarchy	0.5212	0.3881	2.9565

Table 1. Validation results of ViNet with and without hierarchy on DHFIK.

Clip Size ( $T$ )	CC	SIM	NSS
8	0.4978	0.363	2.8221
16	0.5112	0.378	2.9067
32	0.5212	<b>0.3881</b>	<b>2.9565</b>
48	<b>0.5231</b>	0.3807	2.9477

Table 2. Validation results on varying clip size for training ViNet on DHFIK.

for the next layer.  $D_1$  and  $D_5$  consists of 3D convolutional and upsampling layer and  $D_6$ , being the last layer, consists of just 3D convolutional layers.

$D_1$  takes input features from the Backbone network in the case of ViNet or else, takes the output of the fusion block in AViNet. Each upsampling layer increases the spatial dimension by two but keeps the temporal dimension the same. For the next three layers, we perform the following operation

$$O_i = D_i(O_{i-1} \oplus X_{5-i}) \quad \forall i = 2, 3, 4 \quad (2)$$

where  $\oplus$  is concatenation along the temporal dimension. We also perform the concatenation operation along the channel dimension, which is discussed in later sections.  $O_4$  is passed through  $D_5$  to match the spatial dimension with that of the input image. The resulting output is passed through  $D_6$  to collapse the channel and temporal dimension to 1 since we predict a single saliency map. The output is passed through a sigmoid activation function to generate the final saliency map.

$$S = \sigma(O_6) = \frac{1}{1 + e^{-x}} \quad \forall x \in O_6 \quad (3)$$

### 3.4. Evaluation

AViNet follows the sliding window approach to generate a saliency map for all frames in the video. In other words, we predict saliency map  $S_t$  at time step  $t$  by taking  $F_{t-T+1}, \dots, F_t$  sequence of frames as input. Due to this approach, we have to assume that the minimum number of frames in the video should be  $2T - 1$ . If the video’s length is less than  $2T - 1$ , we repeat the first frame of the video and prepend it until the length becomes  $2T - 1$ . The problem with this approach is predicting the first  $T - 1$  saliency maps. So we follow the workaround similar to [24], where we reverse the first  $T$  clips and move in the same manner until the first  $T - 1$  saliency maps are generated. ViNet takes around 0.016 seconds to generate a saliency map.

	DHF1K					Hollywood-2					UCF Sports				
	CC	sAUC	AUC	NSS	SIM	CC	sAUC	AUC	NSS	SIM	CC	sAUC	AUC	NSS	SIM
<b>SALEMA</b>	0.449	0.667	0.890	2.57	<b>0.466</b>	0.613	0.708	0.919	3.18	0.487	0.544	0.740	0.906	2.63	0.431
<b>ACLNet</b>	0.434	0.601	0.890	2.35	0.315	0.623	0.757	0.913	3.08	<b>0.542</b>	0.510	0.744	0.897	2.56	0.406
<b>STRA-Net</b>	0.458	0.663	0.895	2.55	0.355	0.662	0.774	0.923	3.47	0.536	0.593	0.751	0.910	3.01	0.479
<b>SALSAC</b>	0.479	0.697	0.896	2.67	0.357	0.670	0.712	0.931	3.35	0.529	<b>0.671</b>	<b>0.806</b>	<b>0.926</b>	3.52	<b>0.534</b>
<b>TASEDNet</b>	0.470	<b>0.712</b>	0.895	2.66	0.361	0.64	0.768	0.918	3.30	0.507	0.582	0.752	0.899	2.92	0.469
<b>UNISAL</b>	0.490	0.691	<b>0.901</b>	2.77	<b>0.390</b>	<b>0.673</b>	0.795	<b>0.934</b>	<b>3.90</b>	<b>0.542</b>	0.644	0.775	0.918	<b>3.38</b>	<b>0.523</b>
<b>ViNet</b>	<b>0.510</b>	<b>0.728</b>	<b>0.908</b>	<b>2.87</b>	0.381	<b>0.693</b>	<b>0.813</b>	<b>0.930</b>	<b>3.73</b>	<b>0.550</b>	<b>0.673</b>	<b>0.810</b>	<b>0.924</b>	<b>3.62</b>	0.522

Table 3. Comparison results on the DHF1K, Hollywood-2 and UCF-sports test sets. The best scores are shown in red and second best scores in blue.

## 4. Experiments and Results

### 4.1. Datasets

#### 4.1.1 Visual Datasets

The three most popular visual-only datasets in video saliency are DHF1K, Hollywood-2, and UCF-sports. We carry out the tests and comparisons on these three datasets.

DHF1K is a recently collected dataset for video saliency prediction tasks. It contains 1000 videos where 700 videos are for training (100 for validation), and 300 are preserved as the test set with no public ground-truth saliency maps, unlike other datasets. All our experiments and analysis are based on this dataset since it is the most general and diverse dataset as opposed to the other two task-specific datasets.

Hollywood-2 is the largest dynamic eye-tracking dataset consisting of 1707 videos. It is a task-specific dataset which focuses on human actions in movie scenes. We use the standard split of 823 training videos and 884 test videos.

UCF-sports dataset consists of 150 videos focusing on human actions in sports. We use a standard split with 103 videos for training and 47 videos for testing.

#### 4.1.2 Audio-Visual Datasets

There are seven audio-visual datasets in video saliency: DIEM, Coutrot1, Coutrot2, AVAD, ETMD, SumMe, and AVE dataset. We carry out the tests and comparisons on these seven datasets.

DIEM [27] consists of 81 movie clips of varying genres. They sourced from publicly accessible repositories, including advertisements, documentaries, game trailers, movie trailers, music videos, news clips, and time-lapse footage. It consists of 64 training videos and 17 test video.

Coutrot databases [9, 10] are split into Coutrot1 and Coutrot2. Coutrot1 contains 60 clips with dynamic natural scenes split into 4 visual categories: one/several moving objects, landscapes, and faces. Coutrot2 contains 15 clips of 4 persons in a meeting and the corresponding eye-tracking data from 40 persons.

AVAD dataset [25] contains 45 short clips of 5-10 sec duration with several audio-visual scenes, e.g., dancing, guitar

playing, birds singing, etc.

ETMD dataset [18] contains 12 videos from six different hollywood movies.

SumMe dataset [14] contains 25 unstructured videos, i.e., mostly user-made videos, as well as their corresponding multiple-human created summaries, which were acquired in a controlled psychological experiment.

AVE dataset [37] consists of 150 hand-picked video sequences from DIEM, Coutrot-1 and 2 datasets. The videos are divided into three categories - Nature, Social Events, and Miscellaneous. The dataset consists of 92 training videos, 29 validation, and 29 test sequences.

### 4.2. Experimental Setup

For training ViNet, clips with  $T$  consecutive frames were randomly selected from the dataset. Each frame is resized to  $224 \times 384$  and trained on the dataset with a batch size of 8. The optimizer used is Adam, and the learning rate is set to be  $1e-4$ . The network is initially trained on DHF1K dataset. The validation set of DHF1K is used for early stopping. The trained model is then fine-tuned for Hollywood-2 and UCF-sports dataset using their respective training sets. The test sets of Hollywood-2 and UCF-sports are used for early stopping.

For training AViNet, weights of ViNet pre-trained on DHF1K are used and fine-tuned on the audio-visual datasets. For DIEM, the standard split provided in the literature is used. For other datasets, there are no standard splits defined, so we evaluated our model on 3 different splits defined by [39] and report the average metric values across various splits. For evaluating on AVE dataset, we fine-tune the model using its training set and use its validation for early stopping.

### 4.3. Loss Function

We choose the most widely used Kullback-Leibler divergence as the loss function, which is often used in saliency prediction tasks. KLdiv is an information-theoretic measure of the difference between two probability distributions:

$$KLdiv(P, Q) = \sum_i Q_i \log\left(\epsilon + \frac{Q_i}{P_i + \epsilon}\right), \quad (4)$$

	DIEM					Coutrot1					Coutrot2				
	CC	sAUC	AUC	NSS	SIM	CC	sAUC	AUC	NSS	SIM	CC	sAUC	AUC	NSS	SIM
<b>ACLNet</b>	0.522	0.622	0.869	2.02	0.427	0.425	0.542	0.85	1.92	0.361	0.448	0.594	0.926	3.16	0.322
<b>TASENet</b>	0.557	0.657	0.881	2.16	0.461	0.479	0.58	0.867	2.18	0.388	0.437	0.611	0.921	3.17	0.314
<b>STAVISNet</b>	0.579	0.674	0.883	2.26	0.482	0.472	0.584	0.868	2.11	0.393	0.734	0.71	<b>0.958</b>	5.28	<b>0.511</b>
<b>ViNet(NF)</b>	0.571	0.695	0.886	2.28	0.468	0.509	0.619	0.875	2.46	0.406	0.645	0.72	0.949	5.11	0.419
<b>ViNet</b>	0.626	<b>0.723</b>	0.898	2.47	0.483	0.551	0.633	0.886	2.68	0.423	0.724	0.739	0.95	5.61	0.466
<b>AViNet(B)</b>	0.632	0.719	0.899	2.53	0.498	0.56	0.635	0.889	<b>2.73</b>	0.425	<b>0.754</b>	<b>0.742</b>	0.951	<b>5.95</b>	0.493
<b>AViNet(T)</b>	<b>0.637</b>	0.722	<b>0.901</b>	<b>2.54</b>	<b>0.504</b>	<b>0.561</b>	<b>0.638</b>	<b>0.891</b>	2.71	<b>0.427</b>	0.738	0.739	0.953	5.73	0.477
<b>AViNet(C)</b>	0.631	0.720	0.897	2.50	0.497	0.556	0.636	0.887	2.68	0.426	0.753	0.743	0.951	5.81	0.486

Table 4. Comparison results on the DIEM, Coutrot1 and Coutrot2 test sets.

	AVAD					ETMD					SumMe				
	CC	sAUC	AUC	NSS	SIM	CC	sAUC	AUC	NSS	SIM	CC	sAUC	AUC	NSS	SIM
<b>ACL-Net</b>	0.58	0.56	0.905	3.17	0.446	0.477	0.675	0.915	2.36	0.329	0.379	0.609	0.868	1.79	0.296
<b>TASE-Net</b>	0.601	0.589	0.914	3.16	0.439	0.509	0.711	0.916	2.63	0.366	0.428	0.657	0.884	2.1	0.333
<b>STAVIS-Net</b>	0.608	0.593	0.919	3.18	0.457	0.569	0.731	<b>0.931</b>	2.94	<b>0.425</b>	0.422	0.656	0.888	2.04	0.337
<b>ViNet (NF)</b>	0.665	0.651	0.923	3.67	0.501	0.544	0.719	0.924	2.92	0.404	0.455	0.687	0.893	2.35	0.349
<b>ViNet</b>	<b>0.694</b>	<b>0.663</b>	0.928	<b>3.82</b>	<b>0.504</b>	0.569	0.736	0.928	3.06	0.409	0.466	0.696	0.898	2.40	0.345
<b>AViNet(B)</b>	0.674	0.658	0.927	3.77	0.491	0.571	0.733	0.928	<b>3.08</b>	0.406	0.463	0.692	0.897	2.41	0.343
<b>AViNet(T)</b>	0.689	<b>0.663</b>	<b>0.931</b>	3.74	0.499	<b>0.576</b>	<b>0.740</b>	<b>0.931</b>	3.07	0.410	0.470	<b>0.697</b>	<b>0.900</b>	<b>2.42</b>	<b>0.350</b>
<b>AViNet(C)</b>	0.683	0.661	0.931	3.74	0.494	0.566	0.737	0.928	3.05	0.404	<b>0.471</b>	0.699	0.899	<b>2.42</b>	0.346

Table 5. Comparison results on the AVAD, ETMD and SumMe test sets.

where  $P$ ,  $Q$  are predicted and ground truth maps respectively and  $\epsilon$  is a regularization term.

#### 4.4. Ablation studies

**ViNet** We first present ablations studies for the ViNet model. All the ablations in this section are performed with training on the DHF1K training set and evaluation on its validation set. We examine the effects of (a) changing the clip size, (b) using multi-level features, (c) replacing up-sampling with transpose convolutions, and (d) applying different concatenation techniques for margin hierarchy. Table 2 illustrates the results on varying the clip size of the input and using clips of size 32 frames gave the best results. Ablation results by using hierarchical features can be found in Table 1. It clearly indicates that using multi-level features adds up to the performance. We also use transpose convolution instead of trilinear upsampling to increase the spatial dimension, but CC decreased to 0.5178 from 0.5212. The multi-level features extracted from the backbone are concatenated at each decoder block. We tried two ways of concatenating features - across temporal dimension and channel dimension. We observed that they gave a similar performance; therefore, we went ahead with the former approach due to fewer trainable parameters.

**AViNet** We use a similar split as in [39] for ablation studies for audio-visual saliency detection. As already described in 4.2, we use the average over three different splits as the performance measure. AViNet consists of ViNet to encode video information, a sound module to encode audio information, and a fusion block to merge the two modalities’ features.

We applied various fusion methods, namely bilinear concatenation (AViNet (B)), simple concatenation (AViNet (C)), and transformer based fusion (AViNet (T)). The results of the fusion methods are provided in Table 4 and 5. The transformer-based fusion gave slight improvement on metric values across various datasets because of self-attention between audio and visual features. However, the bilinear concatenation method provides a good trade-off between the increase in parameters and the metric values.

#### 4.5. Comparison with state of the art

**Visual only datasets** We quantitatively compare our model with state of the art models on DHF1K, Hollywood-2, and UCF-Sports test set. Table 3 shows the results on all three datasets in terms of CC, sAUC, AUC, NSS, and SIM metrics. We only compare with the existing top six approaches. We can observe that ViNet outperforms all the state of the art models on the DHF1K dataset. ViNet also achieves top results on most metrics on Hollywood-2 and UCF-Sports datasets. At the time of the submission, ViNet is the top-performing model on the DHF1K challenge (evaluated on the private test set).

**Audio Visual Datasets** We also compare AViNet and ViNet on the visual-audio datasets - DIEM, Coutrot 1 and 2, AVAD, ETMD, and SumMe. We compare AViNet against the state of the approaches, ViNet, and the fusion variations of the AViNet model. It is evident from Table 4 and 5 that both AViNet and ViNet outperform state-of-the-art STAVIS-Net by a large margin on all datasets. For visualization purposes, in Fig. 5 sample frames from DIEM are pre-

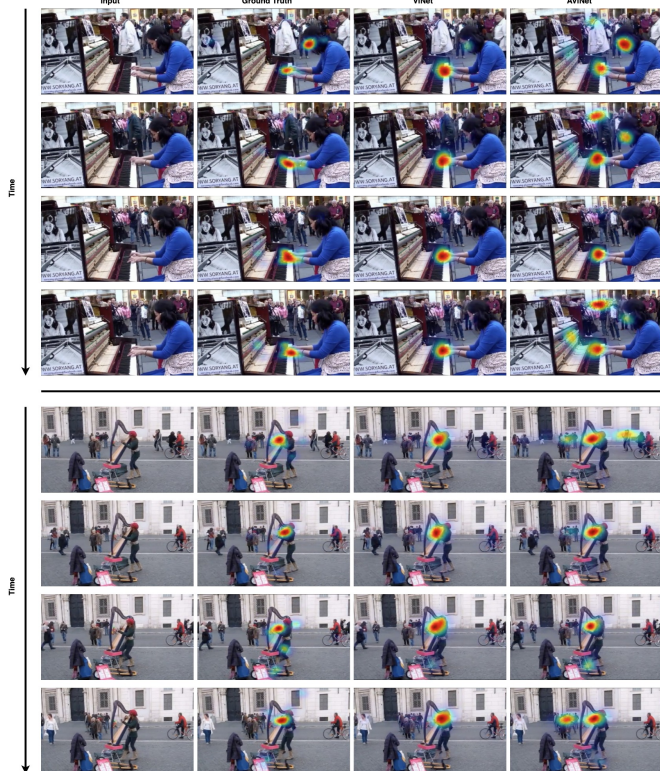


Figure 3. Sample frames from AVAD database [25] with the corresponding ground truth, ViNet and AViNet visual saliency maps for comparison. In both videos, the artist is playing the instrument. ViNet focuses on the action (hand movement) efficiently whereas, AViNet tries to localize the sound of the instrument in the background, thereby diffusing saliency.

sented. It can be easily observed that our results are closer to the ground truth. We observed that Coutrot-2 is the only dataset that had a significant improvement in the Audio-Visual model over the visual-only model, clearly indicating the importance of localizing sound in the social conversations scenario. Fig. 4 shows an example for the same. We also evaluate ViNet (NF) trained on DHF1K dataset on these datasets, and surprisingly, it also gives similar performance to STAViS-Net, suggesting the generalization abilities of the models trained on DHF1K dataset.

However, it must be noted that the Coutrot-2 dataset has a lack of diversity. All its videos are shot at the same place. Our results motivate the need to curate more diverse datasets consisting of social events with people having a conversation in multiple scenarios/scenes/situations. We also notice that the visual model seems to perform better than the Audio-Visual model in the cases where audio doesn't provide any useful information but instead can act as noise and confuse the model. Fig. 3 shows two examples where the audio doesn't play important role in predicting saliency and thereby, generating poor results.

We also evaluate the performance of our models on the

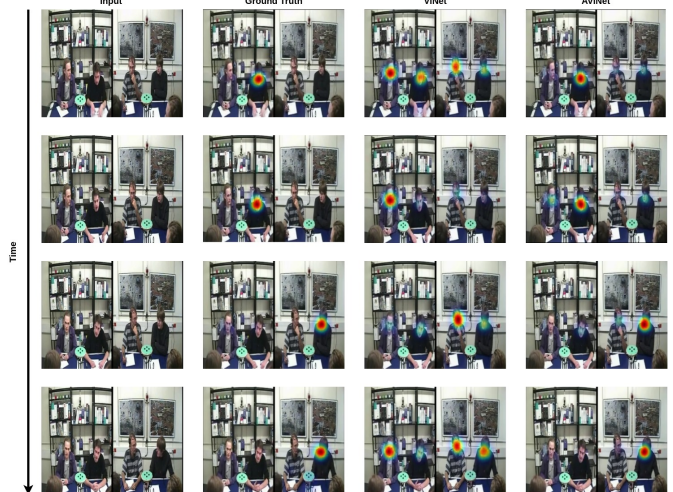


Figure 4. Sample frames from the Coutrot2 [10] dataset with corresponding ground truth, ViNet and AViNet visual saliency maps for comparison. Video shows conversation among four people sitting in the room. ViNet fails to localize the speaker but focuses on the person doing any action while AViNet is able to detect the speaker. Best viewed in color and under zoom.

Cat.	Model Name	CC	sAUC	AUC	NSS	SIM
Nature	HI	0.669	<b>0.762</b>	0.866	<b>3.32</b>	<b>0.538</b>
	AViNet	0.649	0.729	0.895	2.37	0.515
	ViNet	<b>0.680</b>	0.735	<b>0.900</b>	2.47	<b>0.538</b>
	DAVE	0.539	0.723	0.877	2.27	0.450
	ACLNet*	0.517	0.723	0.884	2.03	0.401
Soc Ev.	MEP	0.471	0.686	0.869	1.76	0.368
	HI	0.655	0.759	0.855	<b>3.63</b>	0.516
	AViNet	<b>0.688</b>	<b>0.765</b>	<b>0.914</b>	2.96	0.536
	ViNet	<b>0.688</b>	0.760	0.910	2.88	<b>0.544</b>
	DAVE	0.545	0.726	0.885	2.65	0.442
Misc.	ACLNet*	0.449	0.683	0.869	2.02	0.359
	MEP	0.314	0.633	0.819	1.35	0.274
	HI	0.597	<b>0.748</b>	0.837	<b>3.23</b>	0.481
	AViNet	0.635	0.730	<b>0.898</b>	2.42	0.506
	ViNet	<b>0.636</b>	0.726	0.896	2.40	<b>0.509</b>
Overall	Dave	0.549	0.736	0.881	2.39	0.454
	ACLNet*	0.456	0.683	0.852	1.84	0.378
	MEP	0.438	0.675	0.845	1.73	0.342
	HI	0.644	<b>0.757</b>	0.854	<b>3.41</b>	0.514
	AViNet	0.655	0.744	0.901	2.55	0.516
Overall	ViNet	<b>0.671</b>	0.742	<b>0.903</b>	2.60	<b>0.533</b>
	DAVE	0.545	0.726	0.881	2.45	0.449
	ACLNet*	0.475	0.700	0.870	1.98	0.379
	MEP	0.403	0.662	0.844	1.59	0.326

Table 6. Performance of various models on AVE test set categories. HI represents Human Infinite (HI) represents upper performance bound and Mean Eye Position (MEP) represents lower performance bound.

AVE dataset [37]. Although the AVE dataset is formed using the sequences from DIEM, Coutrot-1, and Coutrot-2 datasets, it is an interesting dataset because (a) it provides a human upper bound and a lower bound using dataset biases and (b) it provides video level categorization. The upper



Figure 5. Sample frames from the DIEM [27] database with the corresponding ground truth, ViNet, AViNet and previous state-of-the-art STAVIS-Net visual saliency maps for comparisons. Both our models are able to capture the salient region (which is the moving honey bee) efficiently whereas STAVIS-Net focuses on the text written and thereby fails to capture the action (movement).

bound is named Human Infinite (HI) and is computed by splitting the eye-movements of observers into two groups and assessing one group against the other (human vs. human performance). The lower bound is called the Mean Eye Position map (MEP) and is computed from the training sequences. It depicts the center-bias that a model may learn by training on the dataset. It is, hence, a robust lower-bound baseline.

AViNet model outperforms the state-of-the-art approaches on the AVE dataset by a significant margin, resonating with the observations on other datasets. However, a highlight point is that AViNet and ViNet models also cross the HI upper bound on AUC-J, CC, and SIM metrics. We further provide a category-wise analysis of both our models on this dataset. It is evident from Table 6 that AViNet seems to perform better than ViNet on videos involving social events like people having a conversation (again, this correlated with the results on the Coutrot-2 dataset). However, on average, the ViNet model outperforms the AViNet. The observation is surprising and contradicts with the findings in previous works [37, 39]. We hypothesize that the observation stems from the fact that the previous models build upon a weak visual-only model.

## 5. Conclusion

We propose ViNet, a novel spatio-temporal visual-only architecture that efficiently addresses the problem of saliency detection in videos. We also propose AViNet by addition of an auditory module to ViNet. We explore three different fusion techniques for combining audio-visual cues. We perform comprehensive analysis of both models on 10 different datasets (3 visual and 7 audio-visual). Our models significantly outperform the state-of-the-art models on

all datasets. The analysis helps to explore the importance of sound cues in video saliency prediction task. We qualitatively compare both our models with each other and observe that visual-only model primarily contributes the underlying performance. Audio-visual saliency would be better espoused with carefully curated datasets.

## References

- [1] Relja Arandjelovic and Andrew Zisserman. Look, listen and learn. In *Proceedings of the IEEE International Conference on Computer Vision*, pages 609–617, 2017. 3
- [2] Relja Arandjelovic and Andrew Zisserman. Objects that sound. In *Proceedings of the European Conference on Computer Vision (ECCV)*, pages 435–451, 2018. 3
- [3] Yusuf Aytar, Carl Vondrick, and Antonio Torralba. Soundnet: Learning sound representations from unlabeled video. In *Advances in neural information processing systems*, pages 892–900, 2016. 2, 3
- [4] Cagdas Bak, Aysun Kocak, Erkut Erdem, and Aykut Erdem. Spatio-temporal saliency networks for dynamic saliency prediction. *IEEE Transactions on Multimedia*, 20(7):1688–1698, 2017. 2
- [5] Loris Bazzani, Hugo Larochelle, and Lorenzo Torresani. Recurrent mixture density network for spatiotemporal visual attention. *arXiv preprint arXiv:1603.08199*, 2016. 2
- [6] Giovanni Bellitto, Federica Proietto Salanitri, Simone Palazzo, Francesco Rundo, Daniela Giordano, and Concetto Spampinato. Video saliency detection with domain adaption using hierarchical gradient reversal layers. *arXiv preprint arXiv:2010.01220*, 2020. 2
- [7] Jin Chen, Huihui Song, Kaihua Zhang, Bo Liu, and Qingshan Liu. Video saliency prediction using enhanced spatiotemporal alignment network. *arXiv preprint arXiv:2001.00292*, 2020. 2
- [8] Yanxiang Chen, Tam V Nguyen, Mohan Kankanhalli, Jun Yuan, Shuicheng Yan, and Meng Wang. Audio matters in



- visual attention. *IEEE Transactions on Circuits and Systems for Video Technology*, 24(11):1992–2003, 2014. 3
- [9] Antoine Coutrot and Nathalie Guyader. How saliency, faces, and sound influence gaze in dynamic social scenes. *Journal of vision*, 14(8):5–5, 2014. 3, 5
- [10] Antoine Coutrot and Nathalie Guyader. Multimodal saliency models for videos. In *From Human Attention to Computational Attention*, pages 291–304. Springer, 2016. 2, 3, 5, 7
- [11] Antoine Coutrot, Nathalie Guyader, Gelu Ionescu, and Alice Caplier. Influence of soundtrack on eye movements during video exploration. 2012. 3
- [12] Richard Droste, Jianbo Jiao, and J Alison Noble. Unified image and video saliency modeling. *arXiv preprint arXiv:2003.05477*, 2020. 1, 2
- [13] Fahad Fazal Elahi Guraya, Faouzi Alaya Cheikh, Alain Tremreau, Yubing Tong, and Hubert Konik. Predictive saliency maps for surveillance videos. In *2010 Ninth International Symposium on Distributed Computing and Applications to Business, Engineering and Science*, pages 508–513. IEEE, 2010. 1
- [14] Michael Gygli, Helmut Grabner, Hayko Riemenschneider, and Luc Van Gool. Creating summaries from user videos. In *European conference on computer vision*, pages 505–520. Springer, 2014. 5
- [15] Hadi Hadizadeh and Ivan V Bajić. Saliency-aware video compression. *IEEE Transactions on Image Processing*, 23(1):19–33, 2013. 1
- [16] Lai Jiang, Mai Xu, and Zulin Wang. Predicting video saliency with object-to-motion cnn and two-layer convolutional lstm. *arXiv preprint arXiv:1709.06316*, 2017. 2
- [17] Ming Jiang, Shengsheng Huang, Juanyong Duan, and Qi Zhao. Salicon: Saliency in context. In *Proceedings of the IEEE conference on computer vision and pattern recognition*, pages 1072–1080, 2015. 2
- [18] Petros Koutras and Petros Maragos. A perceptually based spatio-temporal computational framework for visual saliency estimation. *Signal Processing: Image Communication*, 38:15–31, 2015. 5
- [19] Petros Koutras and Petros Maragos. Susinet: See, understand and summarize it. In *Proceedings of the IEEE Conference on Computer Vision and Pattern Recognition Workshops*, pages 0–0, 2019. 3
- [20] Panagiotis Linardos, Eva Mohedano, Juan Jose Nieto, Noel E O’Connor, Xavier Giro-i Nieto, and Kevin McGuinness. Simple vs complex temporal recurrences for video saliency prediction. *arXiv preprint arXiv:1907.01869*, 2019. 1, 2
- [21] Sophie Marat, Mick el Guironnet, and Denis Pellerin. Video summarization using a visual attention model. In *2007 15th European Signal Processing Conference*, pages 1784–1788. IEEE, 2007. 1
- [22] Marcin Marszalek, Ivan Laptev, and Cordelia Schmid. Actions in context. In *2009 IEEE Conference on Computer Vision and Pattern Recognition*, pages 2929–2936. IEEE, 2009. 2
- [23] Harry McGurk and John MacDonald. Hearing lips and seeing voices. *Nature*, 264(5588):746–748, 1976. 3
- [24] Kyle Min and Jason J Corso. Tased-net: Temporally-aggregating spatial encoder-decoder network for video saliency detection. In *Proceedings of the IEEE International Conference on Computer Vision*, pages 2394–2403, 2019. 1, 2, 4
- [25] Xiongkuo Min, Guangtao Zhai, Ke Gu, and Xiaokang Yang. Fixation prediction through multimodal analysis. *ACM Transactions on Multimedia Computing, Communications, and Applications (TOMM)*, 13(1):1–23, 2016. 3, 5, 7
- [26] Xiongkuo Min, Guangtao Zhai, Jiantao Zhou, Xiao-Ping Zhang, Xiaokang Yang, and Xinping Guan. A multimodal saliency model for videos with high audio-visual correspondence. *IEEE Transactions on Image Processing*, 29:3805–3819, 2020. 3
- [27] Parag K Mital, Tim J Smith, Robin L Hill, and John M Henderson. Clustering of gaze during dynamic scene viewing is predicted by motion. *Cognitive computation*, 3(1):5–24, 2011. 5, 8
- [28] KL Bhanu Moorthy, Moneish Kumar, Ramanathan Subramanian, and Vineet Gandhi. Gazed–gaze-guided cinematic editing of wide-angle monocular video recordings. In *Proceedings of the 2020 CHI Conference on Human Factors in Computing Systems*, pages 1–11, 2020. 1
- [29] Tam V Nguyen, Mengdi Xu, Guangyu Gao, Mohan Kankanhalli, Qi Tian, and Shuicheng Yan. Static saliency vs. dynamic saliency: a comparative study. In *Proceedings of the 21st ACM international conference on Multimedia*, pages 987–996, 2013. 1
- [30] Andrew Owens and Alexei A Efros. Audio-visual scene analysis with self-supervised multisensory features. In *Proceedings of the European Conference on Computer Vision (ECCV)*, pages 631–648, 2018. 3
- [31] Kranthi Kumar Rachavarapu, Moneish Kumar, Vineet Gandhi, and Ramanathan Subramanian. Watch to edit: Video retargeting using gaze. In *Computer Graphics Forum*, volume 37, pages 205–215. Wiley Online Library, 2018. 1
- [32] Navyasri Reddy, Samyak Jain, Pradeep Yarlagadda, and Vineet Gandhi. Tidying deep saliency prediction architectures. *arXiv preprint arXiv:2003.04942*, 2020. 2
- [33] Olaf Ronneberger, Philipp Fischer, and Thomas Brox. U-net: Convolutional networks for biomedical image segmentation. In *International Conference on Medical image computing and computer-assisted intervention*, pages 234–241. Springer, 2015. 2
- [34] Jonas Ruesch, Manuel Lopes, Alexandre Bernardino, Jonas Hornstein, Jos  Santos-Victor, and Rolf Pfeifer. Multimodal saliency-based bottom-up attention a framework for the humanoid robot icub. In *2008 IEEE International Conference on Robotics and Automation*, pages 962–967. IEEE, 2008. 3
- [35] Boris Schauerte, Benjamin K hn, Kristian Kroschel, and Rainer Stiefelwagen. Multimodal saliency-based attention for object-based scene analysis. In *2011 IEEE/RSJ International Conference on Intelligent Robots and Systems*, pages 1173–1179. IEEE, 2011. 3
- [36] Arda Senocak, Tae-Hyun Oh, Junsik Kim, Ming-Hsuan Yang, and In So Kweon. Learning to localize sound source in visual scenes. In *Proceedings of the IEEE Conference*

- on *Computer Vision and Pattern Recognition*, pages 4358–4366, 2018. [3](#)
- [37] Hamed R Tavakoli, Ali Borji, Esa Rahtu, and Juho Kannala. Dave: A deep audio-visual embedding for dynamic saliency prediction. *arXiv preprint arXiv:1905.10693*, 2019. [1](#), [2](#), [3](#), [5](#), [7](#), [8](#)
- [38] Yapeng Tian, Jing Shi, Bochen Li, Zhiyao Duan, and Chenliang Xu. Audio-visual event localization in unconstrained videos. In *Proceedings of the European Conference on Computer Vision (ECCV)*, pages 247–263, 2018. [3](#)
- [39] Antigoni Tsiami, Petros Koutras, and Petros Maragos. Stavis: Spatio-temporal audiovisual saliency network. In *Proceedings of the IEEE/CVF Conference on Computer Vision and Pattern Recognition*, pages 4766–4776, 2020. [1](#), [2](#), [3](#), [5](#), [6](#), [8](#)
- [40] Erik Van der Burg, Christian NL Olivers, Adelbert W Bronkhorst, and Jan Theeuwes. Audiovisual events capture attention: Evidence from temporal order judgments. *Journal of vision*, 8(5):2–2, 2008. [1](#)
- [41] Erik Van der Burg, Christian NL Olivers, Adelbert W Bronkhorst, and Jan Theeuwes. Pip and pop: nonspatial auditory signals improve spatial visual search. *Journal of Experimental Psychology: Human Perception and Performance*, 34(5):1053, 2008. [3](#)
- [42] Argiro Vatakis and Charles Spence. Crossmodal binding: Evaluating the “unity assumption” using audiovisual speech stimuli. *Perception & psychophysics*, 69(5):744–756, 2007. [3](#)
- [43] Wenguan Wang and Jianbing Shen. Deep visual attention prediction. *IEEE Transactions on Image Processing*, 27(5):2368–2378, 2017. [2](#)
- [44] Wenguan Wang, Jianbing Shen, Fang Guo, Ming-Ming Cheng, and Ali Borji. Revisiting video saliency: A large-scale benchmark and a new model. In *Proceedings of the IEEE Conference on Computer Vision and Pattern Recognition*, pages 4894–4903, 2018. [1](#), [2](#)
- [45] Xinyi Wu, Zhenyao Wu, Jinglin Zhang, Lili Ju, and Song Wang. Salsac: A video saliency prediction model with shuffled attentions and correlation-based convlstm. In *AAAI*, pages 12410–12417, 2020. [1](#), [2](#)
- [46] Saining Xie, Chen Sun, Jonathan Huang, Zhuowen Tu, and Kevin Murphy. Rethinking spatiotemporal feature learning: Speed-accuracy trade-offs in video classification. In *Proceedings of the European Conference on Computer Vision (ECCV)*, pages 305–321, 2018. [3](#)